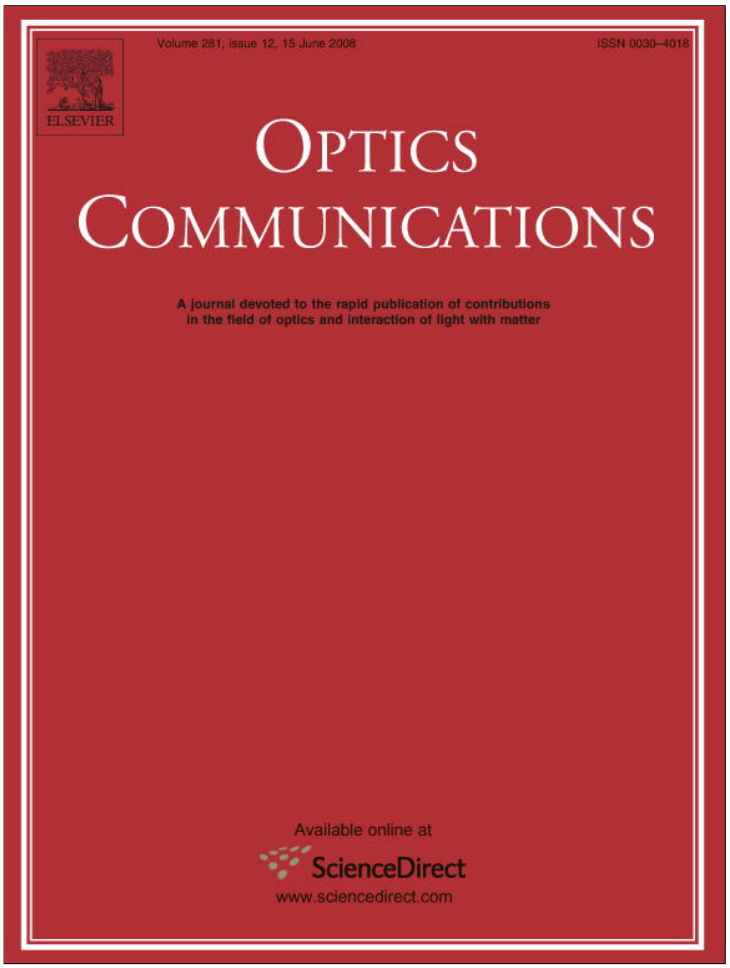

Available online at www.sciencedirect.com
ScienceDirect
Optics Communications 281 (2008) 3375–3380
OPTICS COMMUNICATIONS
www.elsevier.com/locate/optcom

Nonlinear filtering and beam shaping with $\chi^{(3)}$ nonlinear polarization interferometer

S. Kourtev [a,*], N. Minkovski [a], L. Canova [b], O. Albert [b], A. Jullien [b], J. Etchepare [b], S.M. Saltiel [a]

[a] Faculty of Physics, University of Sofia, 5 J. Bourchier Blvd., BG-1164, Sofia, Bulgaria
[b] Laboratoire d'Optique Appliquée, UMR 7639 CNRS, Ecole Polytechnique, ENSTA, 91761 Palaiseau cedex, France

Received 24 August 2007; received in revised form 27 February 2008; accepted 27 February 2008

Abstract

Novel $\chi^{(3)}$-based nonlinear polarization interferometer is theoretically and experimentally investigated. It enables efficient spatial and temporal filtering of femtosecond pulses via generation of cross-polarized wave. By changing the interferometer parameters different beam shapes can be obtained.

PACS: 42.65.Re; 42.70.Mp; 42.60.–v

Keywords: Polarization interferometer; Cross-polarized wave generation; Beam shaping

1. Introduction

Frequency conversion is one of the main application areas of nonlinear optical devices. Nonlinear optical devices are also useful for tuning of various laser beam parameters. With the means of nonlinear optics, one can induce chirp, stretch or compress the pulse, change the polarization properties of the laser radiation, deflect the beam, etc. [1,2]. In particular, it was recently demonstrated that a $\chi^{(3)}$-based cross-polarized wave (XPW) generation device can significantly improve the temporal contrast of femtosecond pulses up to 11 orders of magnitude [3,4]. Here we present an upgrade of the XPW generation setup: a nonlinear polarization interferometer that can be efficiently used for enhancing the XPW generation efficiency, spatial filtering, and beam shaping.

The genuine XPW setup version – a nonlinear crystal placed between crossed polarizers, has been successfully used for femtosecond pulse contrast enhancement [3]. Another XPW generation device constructed by the same elements plus two crossed quarter-wave plates (QWP) has been investigated in [5] towards efficient cross-polarized wave generation.

The proposed here new XPW setup is shown in Fig. 1. It consists of a nonlinear cubic crystal (NLC) placed between two identical quarter-wave plates (QWP1 and QWP2), rotated by the same angle. The nonlinear crystal and the quarter-wave plates are located between two crossed polarizers. This setup corresponds to an unfolded version of the nonlinear mirror [6] previously investigated to demonstrate intensity dependent reflection. The fast axis of the first quarter-wave plate QWP1 is rotated by a relatively small angle α (a few degrees) with respect to the incident polarization direction. This plate splits the input linearly polarized wave into two orthogonally polarized waves (pump and probe) with $\pi/2$ relative phase shift. In the nonlinear crystal the pump produces by $\chi^{(3)}$-effect a XPW signal with a phase-shift of $\pi/2$ with respect to the pump. Therefore, the probe and the generated XPW waves are able to interfere, modifying the amplitude of the probe beam. After the

* Corresponding author.
E-mail address: skourtev@phys.uni-sofia.bg (S. Kourtev).

0030-4018/$ - see front matter © 2008 Elsevier B.V. All rights reserved.
doi:10.1016/j.optcom.2008.02.043

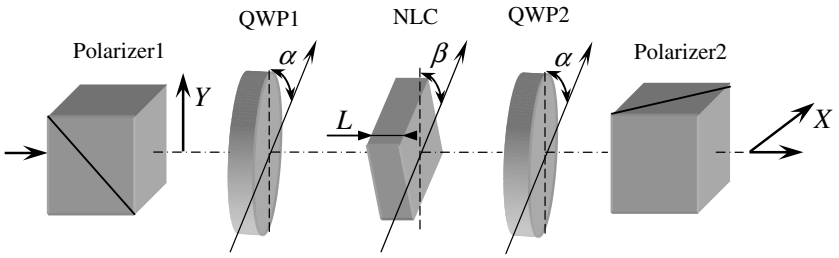

Fig. 1. Scheme of the XPW-based nonlinear polarization interferometer.

second quarter-wave plate QWP2, the pump and the modified probe waves give a single linearly polarized wave. Then, Polarizer2 transmits a wave with polarization perpendicular to the input one, which is called output XPW wave. Because the described device uses the Mach–Zehnder interferometer principle we call it $\chi^{(3)}$ nonlinear polarization interferometer (NPI). The NPI operates in two regimes. In the first one – constructive interference regime, NPI allows improved XPW-efficiency and spatial filtering. In the second – destructive interference regime, various beam shapes can be obtained. We demonstrate both theoretically and experimentally enhanced efficiency of the XPW generation in the NPI due to constructive interference with the XPW-seeding produced by QWP1. We also point out the possibility for spatial beam shaping when using this device in destructive interference regime.

In this paper we show an increased efficiency of XPW generation by comparison with the scheme without quarter-wave plates. We also demonstrate that the transmitted XPW beam can undergo strong spatial shaping depending on the input intensity. The paper is organized as follows. In Section 2, the description of NPI begins with a simple analytical model valid at relatively low intensity, when depletion of the pump wave in the nonlinear crystal can be neglected. The analytical model will provide a good understanding of the involved phenomena. For higher input intensities, a numerical approach is proposed. In Section 3 we investigate beam-shaping properties of the proposed NPI. Experimental results are discussed in Section 4.

2. Theoretical description

2.1. Analytical approach in non-depleted regime

After the QWP1 whose fast axis is rotated by an angle α, the amplitudes of the two waves at the input of the nonlinear crystal are: $A_0(r,t) = D_0(r,t)\cos\alpha$ (along the fast axis of QWP1) and $B_0(r,t) = -iD_0(r,t)\sin\alpha$ (along the slow axis of QWP1). $D_0(r,t)$ is the initial amplitude after the input polarizer. The wave $B_0(r,t)$ is delayed by $\pi/2$ with respect to the wave $A_0(r,t)$, called pump wave. The strong pump wave $A_0(r,t)$ generates in the nonlinear crystal a perpendicularly polarized wave $B(r,t,L)$ [7,8]

$$B(r,t,L) = -i\gamma_\perp L|D_0(r,t)|^2 D_0(r,t)\cos^3\alpha, \quad (1)$$

where $\gamma_\perp = -\gamma_0(\sigma/4)\sin 4(\beta-\alpha)$, $\gamma_0 = (6\pi/8\lambda n)\chi^{(3)}_{xxxx}$, and $\sigma = (\chi^{(3)}_{xxxx} - 2\chi^{(3)}_{xyyx} - \chi^{(3)}_{xxyy})/\chi^{(3)}_{xxxx}$. The two waves $B(r,t,L)$ and $B_0(r,t)$ are in phase and can interfere constructively or destructively depending on the sign of the product $\gamma_\perp \sin\alpha$. The amplitude of the resulting wave $E(r,t,L)$ polarized perpendicularly to the pump wave is

$$E(r,t,L) = -i\left[\gamma_\perp L|D_0(r,t)|^2\cos^3\alpha + \sin\alpha\right]D_0(r,t). \quad (2)$$

After the second quarter-wave plate QWP2 the two orthogonal waves $E(r,t,L)$ and $A_0(r,t)$ will be in phase and will interfere on the polarization plane of the output polarizer (Polarizer2) giving an output field with amplitude $C(r,t) = -A_0(r,t)\sin\alpha - iE(r,t,L)\cos\alpha$. Then the output intensity of the $\chi^{(3)}$ NPI will be proportional to

$$|C(r,t)|^2 = [|D_0(r,t)|\sin 2\alpha + \gamma_\perp L|D_0(r,t)|^3\cos^4\alpha]^2. \quad (3)$$

Expression (3) explains the physical background involved in the NPI. The interference term in (3) consists of two parts: a linear part that depends only on α through $\sin 2\alpha$ and an intensity dependent nonlinear part. They can interfere constructively or destructively depending on the relative signs of $\gamma_\perp$ and $\sin 2\alpha$. If the signs are the same we obtain enhanced XPW-efficiency, while if the signs are opposite the destructive interference leads to beam shaping as we will show below.

For an angle $\alpha = 0$ the output intensity corresponds to the intensity of the device without any quarter-wave plates and contains only the nonlinear term of (3) [7,8]

$$|C_0(r,t)|^2 = [\gamma_\perp L|D_0(r,t)|^3]^2. \quad (4)$$

For $\alpha \neq 0$ the additional linear term $|D_0(r,t)|\sin 2\alpha$ in (3) corresponds to the linear transmission of the NPI. This linear background prevents the NPI device from being used for high temporal contrast improvement.

To calculate the energy conversion efficiency, we integrate (3) over r and t assuming Gaussian spatial and temporal shapes $|D_0(r,t)|^2 = I_0\exp(-2r^2-2t^2)$ where I_0 is the intensity of the input beam at $r = 0$ and $t = 0$. The energy efficiency is defined as the energy ratio between the output XPW pulses and the input pulses

$$\eta_{\mathrm{NPI}} = \int_0^\infty r\int_{-\infty}^\infty |C(r,t)|^2 \mathrm{d}t\mathrm{d}r \Big/ \int_0^\infty r\int_{-\infty}^\infty |D_0(r,t)|^2 \mathrm{d}t\mathrm{d}r. \quad (5)$$

Then the efficiency of XPW generation with NPI becomes:

$$\eta_{\mathrm{NPI}} = \frac{1}{9}\cos^2\alpha(S_\perp^2\sqrt{3}\cos^6\alpha + 9S_\perp\sqrt{2}\cos^3\alpha\sin\alpha + 36\sin^2\alpha), \quad (6)$$

where $S_\perp = \gamma_\perp I_0 L$ $(S_\perp = S(\sigma/4)\ \ \sin4(\beta-\alpha); S = \gamma_0 I_0 L)$. Assuming that $\sigma = -1.2$ for BaF_2 [8,9] we obtain $S_\perp = -0.3S$ for $\beta = \alpha + \pi/8$. The energy efficiency (6) has to be compared with the energy efficiency of the standard (without any QWPs) XPW generator $\eta_0 = \sqrt{3}S_\perp^2/9$.

The comparison of the efficiency of the NPI and the standard XPW generator according to this analytical model is shown on Fig. 2a for angles $\alpha = 6°$ and $\alpha = -6°$. The conversion efficiency of the standard XPW generator corresponds to the case with $\alpha = 0°$.

2.2. Numerical solution

The analytical model provides a simple estimation of the behavior of the $\chi^{(3)}$ NPI. However, this model does not take into account the depletion of the pump beam. To describe the high intensity regime, a numerical approach should be used. Furthermore, the numerical calculations allow to study various spatial and temporal input shapes. The XPW generation process is described by the following equations [5], derived in plane-wave approximation.

$$\frac{dA}{dz} = i\gamma_1|A|^2A - i\gamma_\perp(|B|^2B - A^2B^* - 2|A|^2B) + i\gamma_3(2|B|^2A + B^2A^*), \quad (7a)$$

$$\frac{dB}{dz} = i\gamma_1|B|^2B + i\gamma_\perp(|A|^2A - B^2A^* - 2|B|^2A) + i\gamma_3(2|A|^2B + A^2B^*), \quad (7b)$$

where $\gamma_1 = \gamma_0[1-(\sigma/2)\ \sin^2 2(\beta-\alpha)]$, $\gamma_3 = \gamma_0[(\sigma/2)\sin^2 2(\beta-\ \alpha) + (1-\sigma)/3]$. A- and B-waves are defined in Section 2.1. Group velocity dispersion and diffraction effects are not considered. After solving the Eq. (7) for a given initial spatial and temporal profile $A_0(r,t)$ we find $B(r,t,L)$. Then $A_0(r,t)$ and $B(r,t,L)$ are integrated according to (5) in order to find the conversion efficiency. The input beam entering the NLC is approximated in the numerical simulations with radial amplitude distribution of the form $J_1(r)/r$ where $J_1(r)$ is the first order Bessel function of first kind, which is close to experimental conditions. The temporal shape used in the simulation is secant hyperbolic. The efficiency behavior resulting from the calculations is shown in Fig. 2b.

The general behavior is similar to the analytical case, which points out the validity of the analytical model to describe the involved phenomena. However, the numerical model should yield more accurate results.

We can see that the sign of the product $S_\perp \sin\alpha$ is crucial. For positive $S_\perp \sin\alpha > 0$ (case A on Fig. 2) the XPW efficiency is increased by almost a factor of 4 compared to the original case $\alpha = 0°$. This characteristic could be very useful for XPW applications where a high temporal contrast is not mandatory, as spatial beam filtering or pulse duration reduction [10].

When $S_\perp \sin\alpha < 0$ (case B on Fig. 2), the efficiency presents a minimum value, which was explored in [6] to obtain intensity dependent reflection. In the next section we will underline the ability of this case B to change the spatial profile of the transmitted beam. Furthermore, if the values of the nonlinear index and the anisotropy of the crystal are known, the existence of minimum in curve B can be used for fast estimation of the effective intensity of the beam, which is difficult to measure with sufficient accuracy. On the other hand, if the intensity is known, one can estimate the product of $\chi^{(3)}$ nonlinearity and its anisotropy.

In what follows we focus on spatial beam shaping but notice that similar behavior can be expected for the temporal shape of the pulses.

3. Beam shaping

In destructive interference regime where $S_\perp \sin\alpha < 0$, that corresponds to the case B of Fig. 2, the efficiency is lower but the spatial shape of the transmitted beam exhibits a strong dependence with the input intensity.To demonstrate beam shaping that results from the interference of the probe wave and the generated XPW wave, we first use the analytical model and perform temporal integration

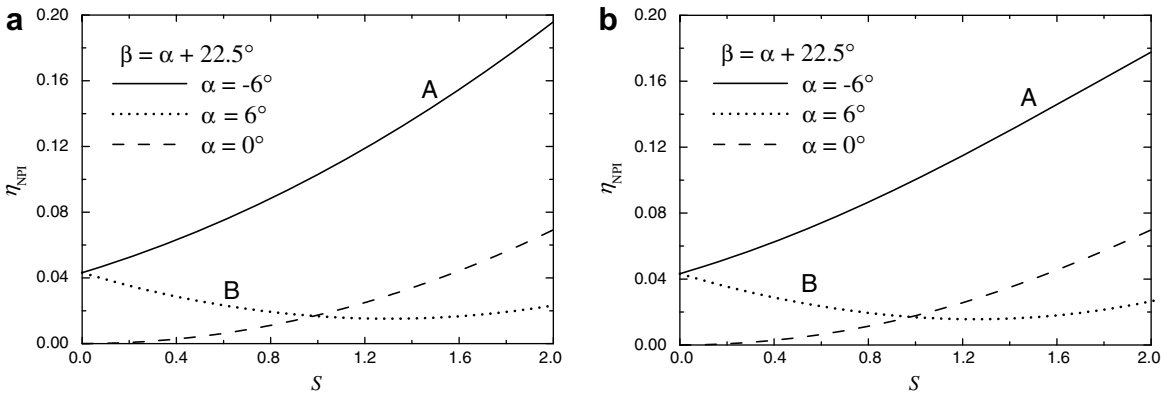

Fig. 2. Calculated efficiency of the NPI using: (a) analytical model (Eq. (6)), and (b) the numerical approach.

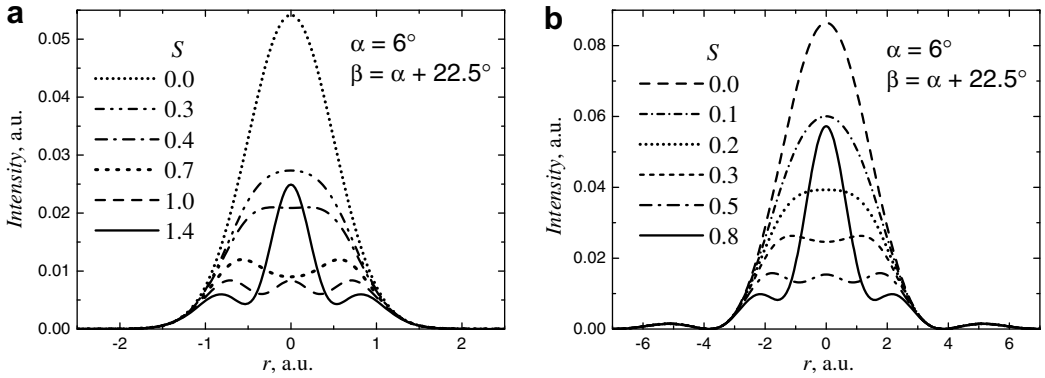

Fig. 3. Different beam profiles obtained using (a) analytical model (Eq. (8)), and (b) the numerical approach.

of (3). The resulting spatial shape of the generated cross-polarized beam is described by

$$B_{\mathrm{XPW}}(r) = \sqrt{\frac{\pi}{6}}\mathrm{e}^{-2r^2}(S_{\perp}^2\mathrm{e}^{-4r^2}\cos^8\alpha + S_{\perp}\sqrt{6}\mathrm{e}^{-2r^2} \times \cos^4\alpha\sin 2\alpha + \sqrt{3}\sin^2 2\alpha). \quad (8)$$

The shapes for $\alpha = 6°$ and different values of the parameter S are shown on Fig. 3a. Beam shapes obtained for the same $\alpha = 6°$ by using the above-described numerical model are presented on Fig. 3b. Generally, the behavior is similar. However the numerical model should give more realistic S-values for each particular beam shape. Different types of spatial shapes can be obtained with the $\chi^{(3)}$ NPI. This beam shaping feature can be advantageous in numerous applications [11,12]. In particular, a smooth top-hat spatial profile is reachable with moderate input intensity value (curves $S = 0.4$ in Fig. 3a and $S = 0.2$ in Fig. 3b), potentially useful for micro-machining applications.

4. Experiments

Experimental setup is shown in Fig. 4. A_1 and A_2 are neutral-density filters. A_1 was used to tune the input energy E_{IN} and A_2 to adjust the intensity of the beam within the dynamic range of the CCD-camera. The NLC was a 2 mm thick z-cut BaF_2 crystal placed in the focus of the L_1 lens ($f = 30$ cm). The lens L_2 with $f = 50$ cm was used to image and magnify d_2/d_1-times the spot of the beam emerging from the BaF_2 crystal onto the CCD sensing area. In the experiment L_2 and CCD were placed in such a way that $d_1 = 54.5$ cm and $d_2 = 528$ cm so the beam spot was magnified 9.7 times in the plane of the CCD. A "Hitachi" KP-M1EK CCD-camera with pixel pitch 11 μm × 11 μm was used to record the beam profile. There was no focusing optics mounted on the camera. The polarizers, the lenses, and the NLC were uncoated.

The laser source was a CPM dye-laser with wavelength 620 nm, pulse duration 100 fs, and repetition rate 10 Hz. In all experiments the maximum input energy was less than 5 μJ. For absolute energy measurements an energy meter was used.

Measured XPW conversion efficiency is shown in Fig. 5. Experimental data are corrected for the reflection losses at uncoated surfaces. The correction factor is chosen so that the averaged transmission of the NPI at very low input intensity to correspond to the theoretical linear transmission due to the presence of the two quarter-wave plates (4.3% transmission for $\alpha = \pm 6°$). Comparison with theoretical behavior calculated with the numerical model is also presented in Fig. 5. Experimental behavior is in good agreement with theoretical predictions. For input energies higher than 1.3 μJ typical saturation of the efficiency was observed. The saturation trend observed in experimental results is due to effects neglected in our theoretical model. At the moment the physical explanation of this early saturation behavior is not known to us. The experimental results confirm that $\chi^{(3)}$ NPI in constructive regime gives higher conversion efficiency ($\alpha = -6°$ in Fig. 5) compared to the standard XPW generator without any quarter-wave

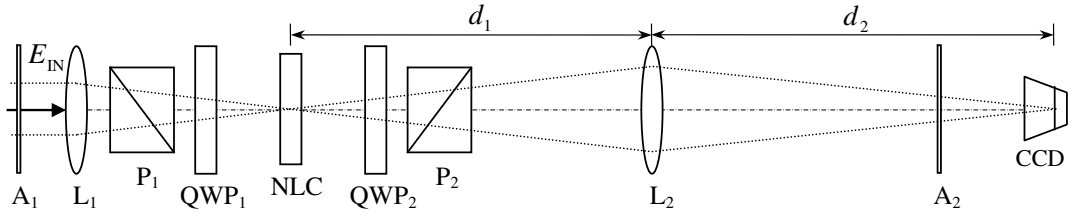

Fig. 4. Experimental setup. A_1, A_2 – attenuation filters; L_1, L_2 – lenses; P_1, P_2 – Glan polarizers; QWP_1, QWP_2 – quarter-wave plates; NLC – BaF_2 crystal; E_{IN} – energy of the input pulses.

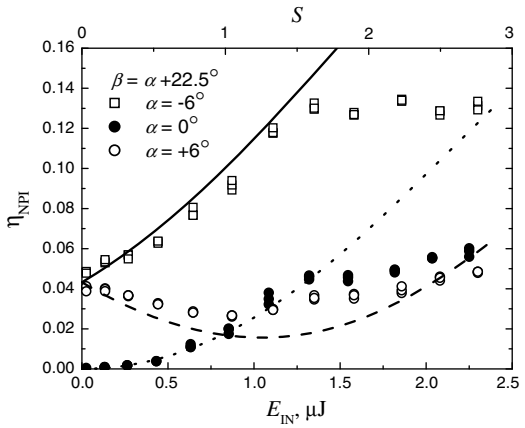

Fig. 5. Experimental dependence of the NPI efficiency on the input energy E_{IN}. Solid, dashed and dotted lines are the theoretical predictions from the numerical model and are plotted as functions of the S-parameter (on the top axis).

plates ($\alpha = 0°$). This setup can consequently represent an interesting more efficient alternative to the standard XPW device.

Beam shaping properties of the device were also investigated for negative product $S_{\perp} \sin \alpha$ (case B). Some beam profiles obtained at different input energies are shown in Fig. 6. For low initial intensity the central part of the beam is mostly converted and for sufficiently high input intensity, the efficiency for the conversion of central part of the beam starts to decrease because of destructive interference. For input energy $E_{IN} = 2.3$ μJ quasi top-hat beam is generated. However, beam profiles from Fig. 6 cannot be directly compared with Fig. 3b profiles as XPW generation is extremely sensitive to the input beam shape, so that any asymmetry in the beam shape like remaining astigmatism is breaking the circular symmetry of the profile.

5. Conclusion

We propose a new Mach–Zehnder type nonlinear polarization interferometer based on $\chi^{(3)}$ cross-polarized wave generation in cubic crystals. Theoretical analysis shows enhanced efficiency of cross-polarized wave generation in constructive regime of the interferometer in comparison to standard schemes for cross-polarized wave generation. In destructive regime various beam shapes can be obtained by changing the input parameters of the interferometer. In this regime the interferometer can be used for rough estimation of incident light intensity assuming only given beam and pulse shapes and without the necessity of knowing the pulse duration and beam size. Potential applications of the beam-shaping capability of this device are: micro-machining, laser ablation, medical applications, optical tweezers, etc. The presented nonlinear polarization interferometer will be useful in applications in which very high temporal contrast improvement is not required but higher efficiency of cross-polarized wave conversion is desired. The experiments that were carried out with the proposed nonlinear polarization interferometer confirmed the theoretically predicted behavior of the device.

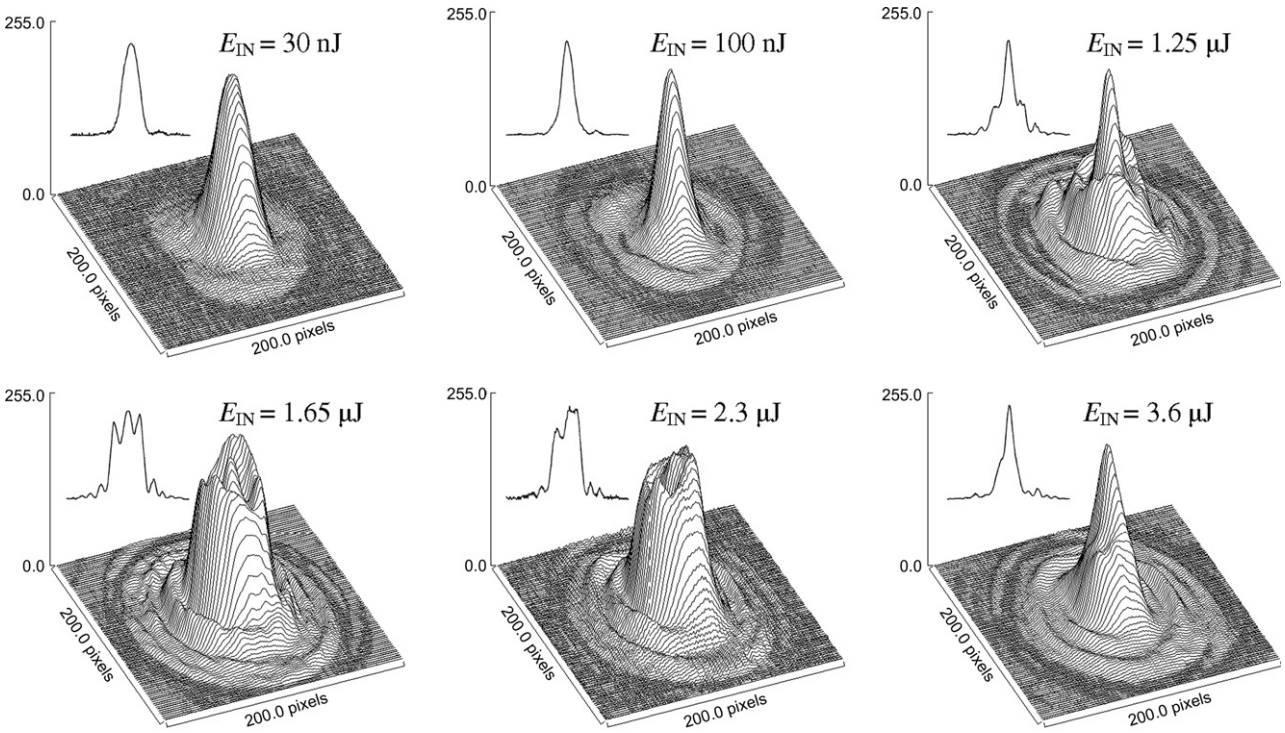

Fig. 6. Experimentally obtained beam profiles at different input energies. Quarter-wave plates were at $\alpha = 6°$ and nonlinear crystal was at $\beta = \alpha + 22.5°$.

Acknowledgments

This work was performed within the program "Access to Research Infrastructure" (LaserLab-Europe, R‖3-CT-2003-506350). S.K., N.M., and S.S. acknowledge the partial support by the Bulgarian National Science Fund through Contract No. IRNI-17.

References

[1] S.A. Akhmanov, V.A. Vysloukh, A.S. Chirkin, Optics of Femtosecond Laser Pulses, American Institute of Physics, Melville, New York, 1992.
[2] Yu.P. Svirko, N.I. Zheludev, Polarization of Light in Nonlinear Optics, Wiley, New York, 1998.
[3] A. Jullien, O. Albert, F. Burgy, G. Hamoniaux, J.-P. Rousseau, J.-P. Chambaret, F. Augé-Rochereau, G. Chériaux, J. Etchepare, N. Minkovski, S.M. Saltiel, Opt. Lett. 30 (2005) 920.
[4] V. Chvykov, P. Rousseau, S. Reed, G. Kalinchenko, V. Yanovsky, Opt. Lett. 31 (2006) 1456.
[5] A. Jullien, O. Albert, G. Chériaux, J. Etchepare, S. Kourtev, N. Minkovski, S.M. Saltiel, J. Opt. Soc. Am. B 22 (2005) 2635.
[6] S. Kourtev, N. Minkovski, S.M. Saltiel, A. Jullien, O. Albert, J. Etchepare, Opt. Lett. 31 (2006) 3143.
[7] N. Minkovski, S.M. Saltiel, G.I. Petrov, O. Albert, J. Etchepare, Opt. Lett. 27 (2002) 2025.
[8] N. Minkovski, G.I. Petrov, S.M. Saltiel, O. Albert, J. Etchepare, J. Opt. Soc. Am. B 21 (2004) 1659.
[9] R. DeSalvo, M. Sheik-Bahae, A.A. Said, D.J. Hagan, E.W. Van Stryland, Opt. Lett. 18 (1993) 194.
[10] A. Jullien, L. Canova, O. Albert, D. Boschetto, L. Antonucci, Y.-H. Cha, J.-P. Rousseau, P. Chaudet, G. Chériaux, J. Etchepare, S. Kourtev, N. Minkovski, S.M. Saltiel, Appl. Phys. B 87 (2007) 595.
[11] F.M. Dickey, S.C. Holswade (Eds.), Laser Beam Shaping. Theory and Techniques, Marcel Dekker Inc., New York, 2000.
[12] G. Molina-Terriza, L. Torner, S. Minardi, P. Di Trapani, J. Mod. Opt. 50 (2003) 1563.